Journal of Applied Polymer Science

Photostabilization of Polypropylene by Surface Modified Rutile-Type TiO_2 Nanorods

Lin Qi,[1] Yanfen Ding,[1] Quanxiao Dong,[1,2] Bin Wen,[1] Feng Wang,[1] Shimin Zhang,[1] Mingshu Yang[1]

[1]Beijing National Laboratory for Molecular Science, Key Laboratory of Engineering Plastics, Institute of Chemistry, Chinese Academy of Sciences, Beijing 100190, People's Republic of China

[2]Beijing Engineering Research Center of Architectural Functional Macromolecular Materials, Beijing Building Construction Research Institute, Co., Ltd., Beijing 100039, People's Republic of China

Correspondence to: M. S. Yang (E-mail: yms@iccas.ac.cn)

ABSTRACT: Rutile-type titanium dioxide (TiO_2) nanorods were prepared, superficially modified and tested for the protection of polypropylene (PP) from the UVB and UVC irradiations. The silica coating blocked the active sites on the nanorods and the following calcination further reduced the amount of surface hydroxyl groups and thus, made the TiO_2 nanorods more efficient against the photodegradation. Compared with spherical TiO_2 nanoparticles, the calcined silica-coated TiO_2 nanorods demonstrated good photostabilization efficiency due to the excellent shielding effect and the improved dispersion of the nanoparticles in PP matrix. When used in combination with the conventional hindered amine light stabilizer (HALS), CHIMASSORB® 944, the surface modified TiO_2 nanorods revealed strong synergistic effect during the photo-oxidation of the PP composites. The capacity of photostabilization was much higher than the combination with the commercial spherical TiO_2 nanoparticles and even higher than the typical HALS photostabilization system containing hindered phenol TINUVIN® 328. © 2014 Wiley Periodicals, Inc. J. Appl. Polym. Sci. **2014**, *131*, 40601.

KEYWORDS: ageing; composites; nanoparticles; nanowires and nanocrystals; polyolefins; surfaces and interfaces

Received 4 November 2013; accepted 14 February 2014
DOI: 10.1002/app.40601

INTRODUCTION

Polypropylene (PP) is one of the most widely used polymers because of its attractive combination of good processability, mechanical properties, and chemical resistance.[1] However, one of the major concerns that continually make difficulties to its versatile application is its low resistance to ultraviolet (UV) irradiation.[2] To prevent the photodegradation, UV absorbers, and UV stabilizers have been commonly used in combination.[3] Commercial UV absorbers, which are generally organic compounds, such as derivatives of benzophenone, benzotriazoles, and esters,[4] are effective but will lose efficiency due to their leaching, migration and consumption during the usage. Traditional UV shields, which are usually inorganic micrometric powders, such as carbon black and talc[5,6] would seriously affect the color and transparency of the products while effectively protecting PP from harmful UV radiation. For those reasons, recent research works are focused on novel inorganic UV absorbers at the nanoscale, especially, nanometric metal oxides.[7–16]

As one of the most important metal oxides and semiconductors, titanium dioxide (TiO_2), which exhibits excellent photoactivities, e.g., UV absorbance, and photocatalysis, has been becoming the mainstream and attracting numerous research.[7,16,17] The photochemical activity of anatase- and rutile-type TiO_2 has been well investigated involving many polymers, including polypropylene,[3,18] polyethylene,[19,20] polystyrene,[21] polyurethane,[22] and alkyd/acrylic-based paints/coatings.[23,24] Previous research have demonstrated that the crystalline form, size, and surface property of TiO_2 affected significantly the photocatalytic activity of TiO_2 and the photostabilization of the polymer matrix. For instance, TiO_2 particles in anatase crystalline form revealed higher photocatalytic activity than rutile form, while appropriate surface treatments demonstrated notable influences in lowering the photocatalytic activity of TiO_2.[23] In comparison with the micrometric powders, the nanometric TiO_2 particles have broader prospects considering their lower influence to the color and transparency of polymers.

In addition, the shape of TiO_2 particles also causes different effects on their catalytic activity, photo-induced electron transport, and absorption and desorption to oxygen, and so on. Therefore, much work was committed to prepare anatase nanoparticles with different shape, such as nanodots, nanorods, nanowires, nanotubes, and nanomaterials with mesoporous/nanoporous structures.[17] However, not much research work has

been done on the shape effects of rutile nanoparticles, although they are also widely used in polymeric materials.

Beside the photocatalytic activity, there are other reasons to choose rutile-type TiO_2 as photoaging improver rather than anatase. Because the band gap energy of rutile (3.00 eV) is smaller than that of anatase (3.21 eV), the wavelength region for UV absorption of rutile is broader than anatase.[25] On the other hand, the crystal structure stability and surface integrity of anatase is lower than those of rutile.[25,26] Therefore, rutile-type TiO_2 is preferred.

The synergistic/antagonistic effects between TiO_2 and hindered amine light stabilizers (HALS) are also a complex issue.[3,23,27–29] To provide optimal protection to polymers, the UV stabilizers, UV absorber and antioxidants are often used in combinations.[3] However, the efficiency of HALS reduces significantly due to their adsorption on other additives or fillers present in the polymer.[30,31] Furthermore, some additives (e.g., halogenated flame retardants that are used for fire safety) can react with HALS and directly lead to its invalidity.[32] Therefore, the synergistic/antagonistic effects between TiO_2 and HALS have been analyzed in specific systems. For example, Allen et al.[3,27] found that during photo-oxidation of PP films the rutile pigment was synergistic in stabilization with phenolic antioxidants and HALS, but antagonistic with benzotriazole and benzophenone absorbers. Anatase TiO_2 in combination with HALS was found to be strongly antagonistic, whilst no significant synergy was observed between rutile TiO_2 and HALS in various water and oil-based paint media.[23] In short, it is necessary to do further research on the synergistic/antagonistic effects.

The UV radiation is generally classified into three regions as UVA (wavelength 320–400 nm), UVB (290–320 nm), and UVC (<290 nm).[33] All UV lights are mutagenic or carcinogenic to living creature and harmful to polymers by causing serious breakage of chemical bonds, with the shorter wavelengths being more severe.[33,34] Though UVB and UVC are more destructive, they were less investigated in sunscreen for human being and photostabilization for polymers, because they were normally considered not cross the stratosphere due to its absorbance within the ozone layer.[35] For this reason, most research on photodegradation of polymers have been conducted under UVA and UVB, while the photoageing under UVC was tested on polymers as stable as polyethylene for purpose of accelerated process only in few literatures.[23] However, the ozone depletion or thinning, which have been observed and become grave issue nowadays in some geographic regions, may contribute to the delivery of UVB and UVC onto the surface of the Earth.[35–37] Although the intensity of UVB and UVC on the surface is much weaker than UVA, the degradation of polymer will be significant because the high photon energy enhances dramatically photochemical reactions. Therefore, it is of great importance to study the photoaging process of polymers exposed to UVB and UVC radiation. The other reason to choose UVC as a radiation source in present work is that the degradation rate of PP/TiO_2 composites is more suitable for getting more clear results than UVA and UVB in limited period.

In this work, TiO_2 nanorods with rutile crystalline structure have been synthesized, superficially modified and comprehensively characterized. The nanorods have been tested for the photostabilization of polypropylene upon UV irradiations in comparison with the usual spherical TiO_2 nanoparticles and in combination with an HALS antioxidant. The experimental results have demonstrated that, as a photostabilizer, the rutile TiO_2 nanorods are more efficient than the counterparts.

EXPERIMENTAL

Materials

TiO_2 nanorods (T) were prepared by hydrolyzing $TiCl_3$ (minimum 15 m/m% in HCl solution, containing 5–10% free acid as HCl, Sinopharm Chemical Reagent Co.) according to the method previously reported.[38] Silica-coated TiO_2 nanorods (ST) were obtained using the Stöber method by base-catalyzed hydrolysis of tetraethyl orthosilicate (Sinopharm Chemical Reagent Co.) in isopropanol,[38,39] at a fixed formulation with the TiO_2/SiO_2 ratio of 1 : 1. ST was further calcined at 800°C for 1 h to perfect the silica shell on the TiO_2 core and is termed as CST. Spherical TiO_2 nanoparticles, HTTiP-E50 (abbreviated as E50), purchased from the Nanjing High Technology Nano Material Co., were treated with the same procedures to CST (denoted as CS-E50) and used as the reference samples.

Additive-free polypropylene (PPH-XN-N45), with an MFI of 4.8 g per 10 min (230°C and 1.26 kg load), was supplied in powder form by China National Petroleum Corporation. The hindered amine light stabilizer (HALS), poly[[6-[(1,1,3,3-tetramethylbutyl)amino]-1,3,5-triazine-2,4-diyl][(2,2,6,6-tetramethyl-4-piperidyl)imino]-1,6-hexanediyl[(2,2,6,6-tetramethyl-4-piperidyl)imino]] (CHIMASSORB® 944, denoted as C944 hereafter), and the hindered phenol UV absorber, 2-(2H-benzotriazol-2-yl)-4,6-ditertpentylphenol (TINUVIN® 328, denoted as T328 hereafter), were obtained from Ciba Specialty Chemicals, China. The antioxidants Irganox® 1010 and Irgafos® 168 were used as processing stabilizers and added to each composite formulations 0.2 and 0.1 wt %, respectively.

Sample Preparation

PP composites containing TiO_2 nanoparticles and/or additives were prepared by melt blending in an internal mixer equipped on a HAAKE Polylab OS RheoDrive 7 (Thermo Fisher Scientific, Germany) at 170°C with a low rotor speed of 10 rpm for the first 1 min for preheating, then with a high rotor speed of 50 rpm for another 6 min blending. Sample films (30–50 μm in thickness) were obtained by hot pressing the composites at 200°C with a pressure of 10 MPa. The concentration of TiO_2 nanoparticles was fixed at 0.5 wt % unless otherwise stated. The contents of C944 and T328, if used, were 0.3 wt % for each.

Photodegradation

The photodegradation of the various PP composites was carried out upon UVB and UVC irradiations at 40°C in air in a CL-1000 Ultraviolet Crosslinker (UVP LLC) for different periods in the range of 0–400 h. The applied UVB radiation was from G8T5/OF lamps (Osram Germicidal) with peak emission at 302 nm while the UVC source was G8T5E bulbs (Ushio) with peak emission at 254 nm. The composite samples were placed 12 cm away from the light source with an exposure of 80,000 μJ cm^{-2}.

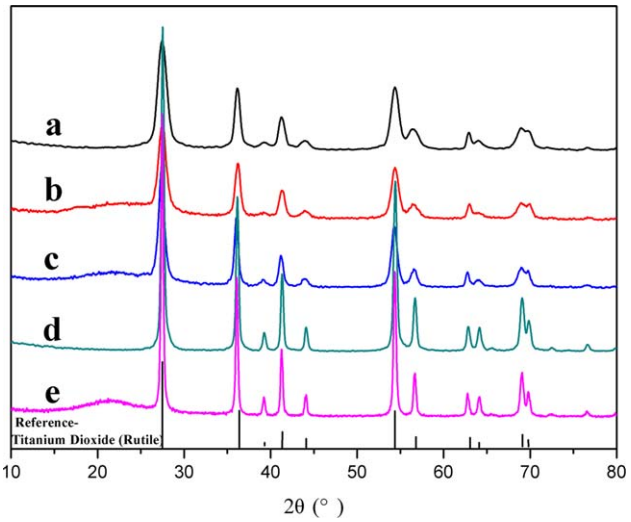

Figure 1. XRD patterns of nanoparticles: (a) T, (b) ST, (c) CST, (d) E50, and (e) CS-E50. The bars on the *X* axis are the characteristic diffraction peaks of rutile standard (JCPDS 21–1276). [Color figure can be viewed in the online issue, which is available at wileyonlinelibrary.com.]

Characterizations

Powder X-ray diffraction (XRD) measurements were performed on a Rigaku (Rigaku Corp.) *D*/max 2400 powder diffractometer with Cu-Kα radiation ($\lambda = 0.154$ nm, 40 kV, 120 mA) at room temperature. The scanning rate was set at 10° min^{-1}.

Transmission electron microscopic (TEM) images of the samples were obtained using a 2200FS high resolution TEM (JEOL) operating at an accelerating voltage of 200 kV.

For the polymer films, Fourier transform infrared (FTIR) spectra were obtained in transmission mode using a Nicolet Avatar 6700 FTIR Spectrometer (Thermo Fisher Scientific Inc.) in the wavenumber range of 4000–650 cm^{-1} and were signal averaged over 16 scans at a resolution of 4 cm^{-1}. Carbonyl groups were easily detected in the broad infrared region at 1800–1680 cm^{-1} for oxidized PP films. To minimize deviations from sample thickness, the peak at 2722 cm^{-1}, which is associated with CH bending and CH_3 stretching,[40] was used as an internal reference in this work. The carbonyl growth was expressed by carbonyl index (CI):

$$CI = \frac{A_{C=O}}{A_{2722}} \quad (1)$$

where $A_{C=O}$ and A_{2722} were the absorbance of carbonyl and the internal reference, respectively. For the nanoparticles, the spectra were obtained in ATR (attenuated total reflection) using the same instrument with a Nicolet Smart Orbit Accessory (Thermo Fisher Scientific).

Thermogravimetric analysis (TGA) was performed on a Pyris 1 apparatus (PerkinElmer) to measure the thermal behavior of the nanoparticles in nitrogen atmosphere from 50 to 750°C at a heating rate of 20°C min^{-1}.

Brunauer–Emmett–Teller (BET) specific surface area was determined using nitrogen adsorption-desorption (77K) and the BET algorithm on a Micromeritics ASAP 2010 surface area and porosity analyzer (Micromeritics Instrument Corporation).

UV–Vis diffuse reflection spectra (DRS) were recorded using a Pgeneral TU-1901 UV–Vis spectrophotometer (Beijing Purkinje General Instrument Co.). Baseline correction was done using a calibrated sample of barium sulfate. UV–Vis transmission spectra of the polymer films were recorded with a UV-2600 UV–Vis spectrophotometer (Shimadzu Corporation). Film thickness was controlled at 50 ± 1 μm for ensuring comparable results.

RESULTS AND DISCUSSION

Characterizations of TiO_2 Nanoparticles

As shown in the XRD pattern (Figure 1), the bare TiO_2 nanoparticles were completely of rutile form and the surface modification did not alter the crystalline form. The average crystallite sizes were calculated from the peak of (101) reflection using Scherrer equation:[41]

$$D = \frac{0.9\lambda}{\beta\cos\theta} \quad (2)$$

where D is the crystallite size, λ is wavelength of the radiation, θ is the Bragg's angle, and β is the full width at half maximum of the (001) peak.

As shown in Table I and Figure 2(a), the bare TiO_2 nanorods (T) had larger BET specific surface area and less agglomerated than others. They were in rod shape with a narrow size distribution and their average size was about 43 nm in length and 9 nm in width, which were quite different from the crystallite size calculated by Sherrer's equation because of their nonspherical shape.[41] For the silica-coated TiO_2 (ST) and calcined silica-coated TiO_2 (CST), no peak of SiO_2 crystals was observed from the XRD patterns (Figure 1), suggesting that the silica coatings were amorphous. From the TEM images [Figure 2(b,c)], the coating layer was estimated to be about 3 nm thick, meanwhile the nanorods were slightly agglomerated. As results, the particle

Table I. BET Surface Area and Particle Size of Nanoparticles Used in this Study

Sample	Crystallite size by Sherrer's equation (nm)	Particle size from TEM images (nm)	BET specific surface area (m^2 g^{-1})
T	17.5	$(43 \pm 12) \times (9 \pm 1)$	154.9
ST	19.5	$(50 \pm 11) \times (15 \pm 2)$	98.5
CST	24.1	$(50 \pm 11) \times (15 \pm 1)$	59.8
E50	42.7	40 ± 16	18.1
CS-E50	50.9	50 ± 15	5.0

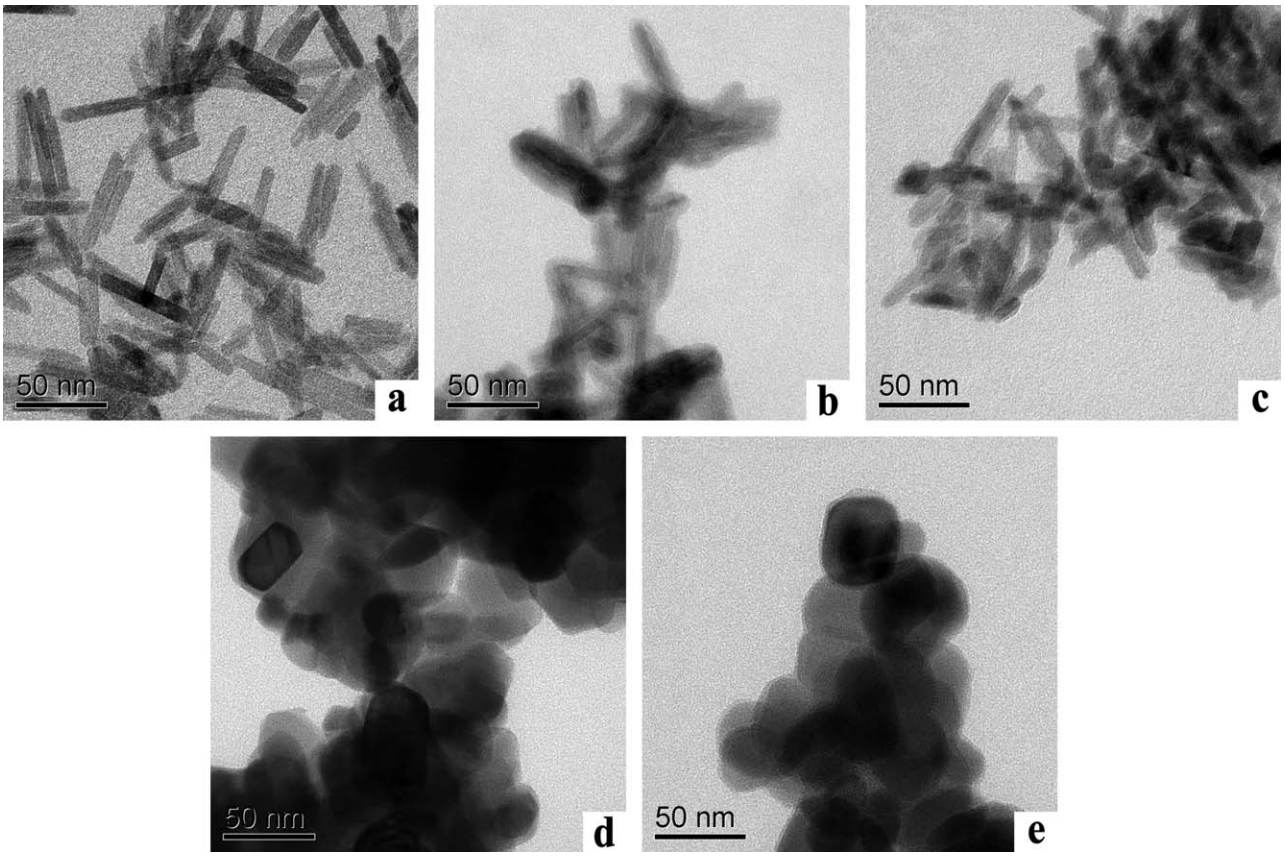

Figure 2. TEM micrographs of nanoparticles: (a) T, (b) ST, (c) CST, (d) E50, (e) CS-E50.

size of the coated TiO_2 increased (in agreement with Sherrer's equation) and the BET specific surface area decreased (Table I). The reference TiO_2 nanoparticles, E50 and CS-E50, revealed low BET specific surface area and large thickness of coating layer because of their spherical shape and more agglomeration [Figure 2(d,e)].

The surface properties, especially the hydroxyl groups, play a major role in controlling the photoactivity and dispersion ability of TiO_2 nanoparticles in polymer matrix.[26,42] FTIR spectroscopy was used to characterize the species on the nanoparticle powders, as shown in Figure 3(a). Evident absorptions of hydroxyl groups were observed on the bare and silica-coated TiO_2 (T and ST). The free and hydrogen bonded OH groups were detected in the region of 3000–3700 cm^{-1} while H—O—H bending were observed in 1600–1700 cm^{-1}, suggesting that the nanoparticles were high hydrophilic. The hydrophilicity of nanoparticles will play a complex role in photodegradation of nonpolar polymer matrix. If the surface hydroxyl groups on the silica shell can be eliminated, the photostability and dispersion ability would be all enhanced.

For this purpose, different calcination conditions were examined. As observed on the TGA curve, there was an obvious weight loss in 500–600°C for ST [Figure 3(b)], which is attributed to the further condensation of silanol, resulting in the formation of more Si—O—Si bonds in the silica coating. To effectively remove the vast majority of the active groups, the calcination of ST was performed on 800°C for 1 h. Under such a condition, the structure of TiO_2 was not damaged. After calcination, the hydroxyl absorption peaks of CST in FTIR were almost completely disappeared [Figure 3(a)] while the crystalline form was maintained in rutile type (Figure 1).

As shown in Figure 4, the UV–Vis DRS curves indicate that all of the rutile-type TiO_2 species had strong absorption to UV light covering almost the full ultraviolet regions from 400 nm down to the acquisition limit of 200 nm.

Dispersion of TiO_2 Nanoparticles in PP Matrix

TEM images of the PP nanocomposites with different nanoparticles are shown in Figure 5. These nanocomposites contained the same amount of TiO_2 (0.5 wt % of the PP matrix). As can be seen from the TEM images, T and ST seemed to have a few large agglomerates in PP matrix due to the high surface hydrophilicity, while CST and CS-E50 were well dispersed. It was observed that the aggregation of nanoparticles was largely reduced after calcination, because the calcination could effectively remove the surface hydroxyl groups on the nanoparticles and improve the silica shell; thus, further improve the dispersion of nanoparticles in the nonpolar polypropylene matrix.

Influence of TiO_2 Nanoparticles on the Photodegradation of PP

To investigate the influence of different nanoparticles on the photostabilization of PP, the films of PP nanocomposites were exposed under the UVC and UVB irradiations respectively for different periods. The pure PP specimens were completely

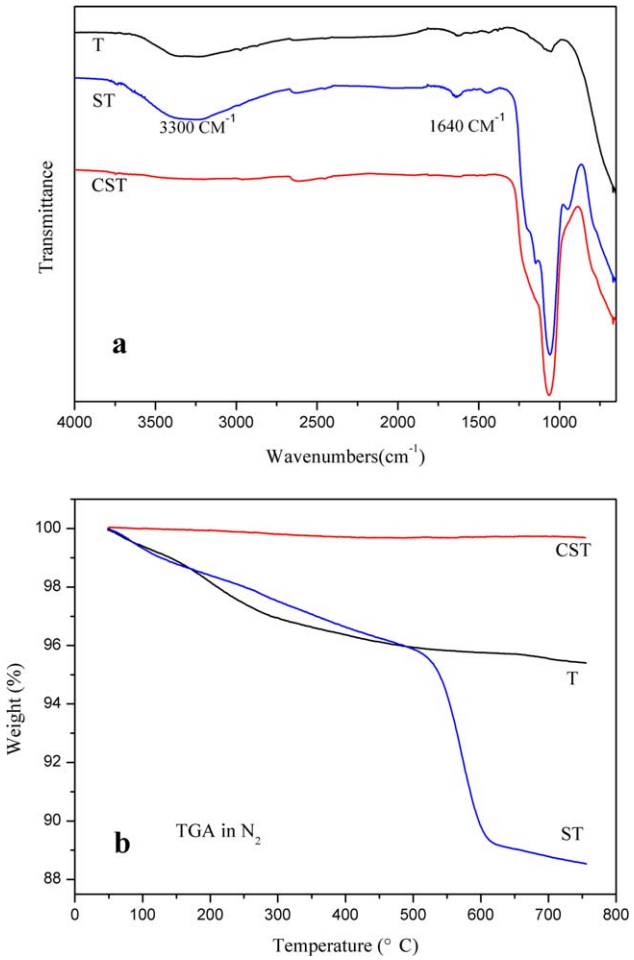

Figure 3. (a) FTIR and (b) TGA (in N_2) curves of the TiO_2 nanorods. [Color figure can be viewed in the online issue, which is available at wileyonlinelibrary.com.]

broken after 160 h exposure under the UVC, while the tests under the UVB could be lasted to 400 h. It confirmed that UVC was more destructive to PP than UVB.

The photodegradation behaviors were characterized by carbonyl index (CI).[43,44] The increases of carbonyl index in PP nanocomposites upon the UV irradiation are shown in Figure 6. The CI curves were concave upwards under the 254 nm shortwave radiation, indicating a significant auto-acceleration for all the tested samples. However, the auto-acceleration was less evident under the 302 nm midwave radiation. In addition, the uncoated TiO_2 accelerated the photodegradation of PP, regardless the wavelength of the radiation exposed. The CI curves of PP/ST were below PP, indicating that the photocatalytic activity of the ST nanorods was effectively suppressed by the silica coating. The calcined silica-coated titanium dioxide nanorods (CST) were the most efficient antiphotoaging agent, revealing efficiency much higher than the spherical counterpart (CS-E50).

The UV–Vis absorption properties of nanocomposites films were also tested. For instance, Figure 7 shows the UV–Vis transmission spectra of the PP films with calcined silica-coated nanoparticles (CST and CS-E50) as well as the bulky PP film.

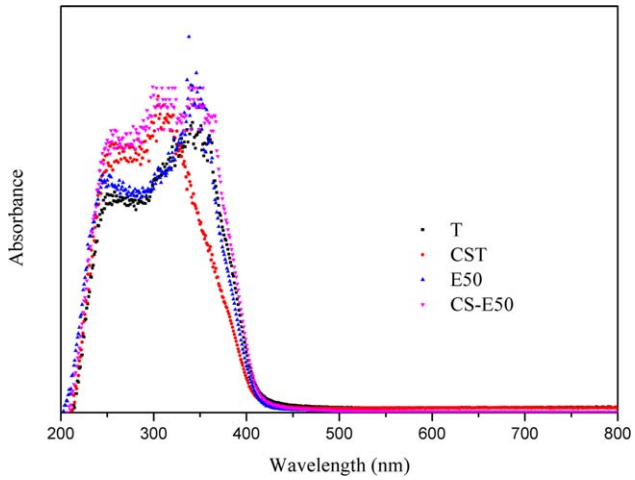

Figure 4. UV–Vis diffuse reflection spectra of the nanoparticles. [Color figure can be viewed in the online issue, which is available at wileyonlinelibrary.com.]

The PP film showed transmittance higher than 80% along the entire UVB range and 70% around 254 nm UVC. In the same wavelength range, CST was able to cutoff a large fraction of the UV radiation. Although the TiO_2 content in nanocomposites was rather small (0.5 wt % of PP) and the films were quite thin (about 50 μm thick), for wavelengths lower than 320 nm, it is notable that the transmission intensity of PP/CST was reduced to 10–20%.

The UV blocking performance of PP/CS-E50 was clearly unsatisfactory. On one hand, its UV shielding efficiency was relatively low (less than 50% UV radiation was blocked). On the other hand, its absorption of visible light made a negative impact on the transparency of PP films. As discussed above, although most of CS-E50 nanoparticles were dispersed at the nanoscale level (Figure 5), the agglomeration of these spherical particles seemed to have serious reduction on effective shielding area which would lead to poor UV-shielding property of the PP composites.

As a conclusion, the present work have demonstrated that the CST nanorods had high efficiency of protecting PP from harmful UV radiation because of the good dispersion in PP matrix and the improved photostability of the silica shell. The following discussion will focus on the combinations of the CST nanorods with the light stabilizer CHIMASSORB® 944 in comparison with the organic UV absorber TINUVIN® 328.

Combinations of CST Nanorods with HALS

As a typical HALS used in polymers, CHIMASSORB® 944 exhibits good thermal stability and resistance to extraction. It has excellent compatibility with PP and can improve greatly the light stability of PP and thus has been widely used in commercial. In this work, TiO_2 nanoparticles were used in combination with CHIMASSORB® 944 to achieve a better light protection to PP.

The influence of CST content in the PP/C944/CST combination was tested by fixing the C944 content as 0.3 wt %, which was the commonly used concentration in PP,[45] and changing the

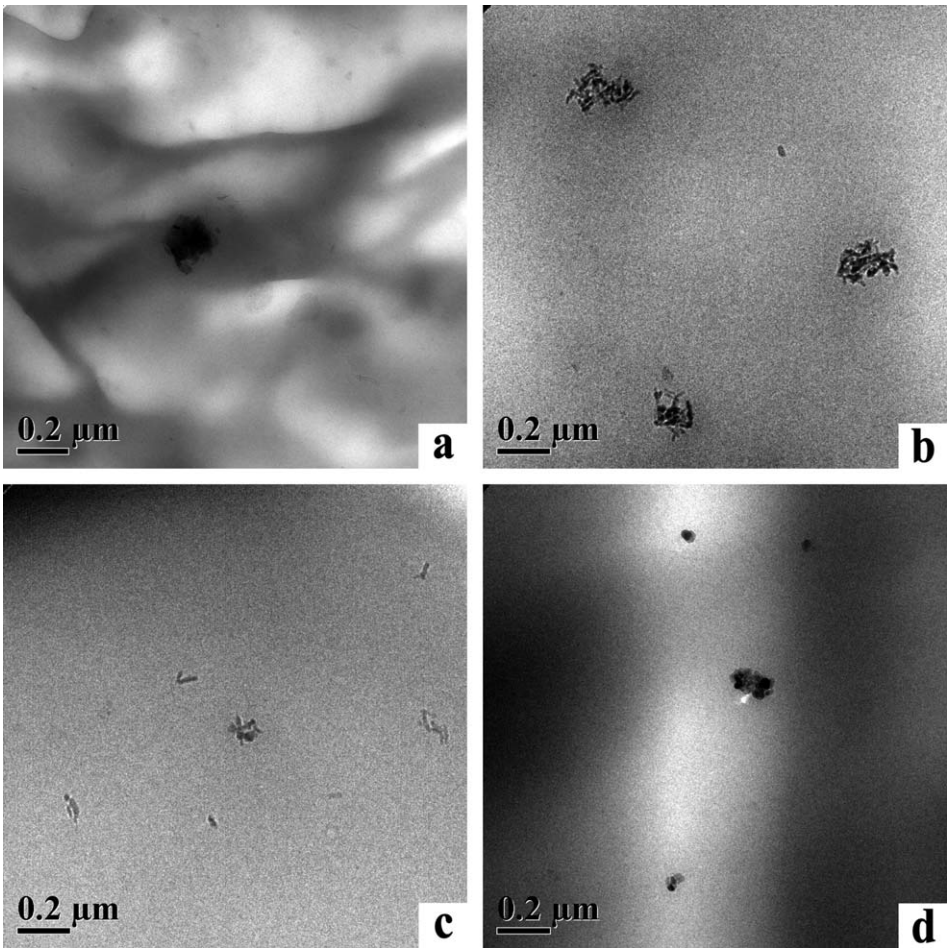

Figure 5. TEM images of (a) PP/T, (b) PP/ST, (c) PP/CST, and (d) PP/CS-E50.

TiO_2 content from 0.1 to 0.5 wt %. As shown in Figure 8, the PP/C944/CST nanocomposites showed a longer induction time and weaker auto-acceleration rate than the PP/C944 blend. A synergistic effect was found between CST and C944 during photodegradation of PP: For both the 254 and 302 nm radiations, the increment of carbonyl index [CI(t)-CI(0)] reduced greatly when the CST content increased from 0 to 0.3 wt %, but varied slightly as the CST content increased from 0.3 to 0.5 wt %.

For comparison, the spherical CS-E50 nanoparticles were used in the combination instead of the CST nanorods and tested for photo-oxidation under the same conditions. The results are shown in Figure 9. It is seen that the CI values of PP/C944/CS-E50 were intermediate between PP/C944/CST and PP/C944, suggesting that, comparing to the rod-like CST, the spherical nanoparticles had a similar, but weaker synergistic effect with the C944. As discussed above, the CST nanorods had larger BET specific surface area, higher aspect ratio and better shielding ability than the spherical CS-E50 and therefore, revealed reduced carbonyl index in the PP/C944/CST combinations. In other words, the PP/C944/CST nanocomposite had better photostability than the PP/C944/CS-E50 nanocomposite.

TINUVIN® 328 (T328) is a commercial hindered phenol UV absorber and was designed for coatings. It is also commonly used in combination with HALS for light stabilization to polyolefins[46–48] and thus was chosen for UV absorbing and antiaging in comparison with PP/C944/CST. The carbonyl index curves of oxidation of the corresponding samples are given in Figure 10. In the presence of the CST nanorods, the carbonyl index of PP/C944/CST increased slowly than the PP/C944 blend; it is to say, the CST nanorods had a positive effect on the stabilization of PP. The carbonyl index of PP/C944/CST were lower than that of PP/C944/T328 upon the exposure time, indicating that the stabilization efficiency of CST with C944 was superior to the hindered phenol. Overall, the advantage of CST over T328 was more evident under the 254 nm radiation than 302 nm, suggesting that the nanorods were more efficient under the more harmful shortwave UV.

Direct spectrometric measurements of UV attenuation (Figure 11) showed that about 75% of the radiation was cut off with the film containing CST and C944. In comparison, the PP film containing the same amount of T328 and C944 absorbed less than 70% of the radiation. This was in agreement with the different UV-absorption mechanisms of TiO_2 and T328. The rutile-type TiO_2 is a semiconductor with a wide band gap energy of 3.0 eV and could absorb photons of electromagnetic radiation with energy greater than the band gap, equivalent to

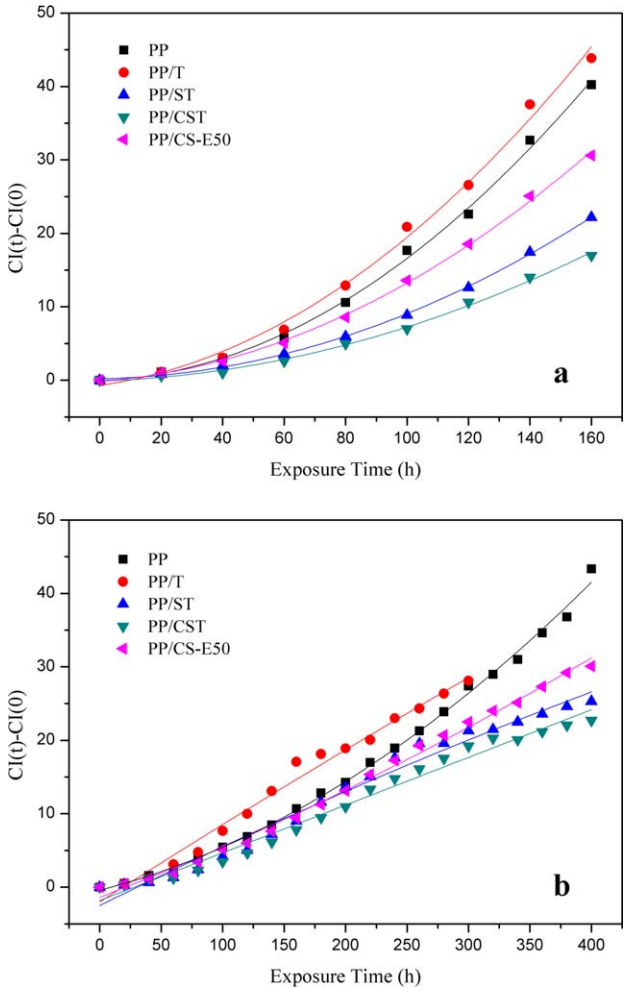

Figure 6. Carbonyl index of PP nanocomposites (0.5 wt % TiO_2) under (a) UVC (254 nm) and (b) UVB (302 nm). [Color figure can be viewed in the online issue, which is available at wileyonlinelibrary.com.]

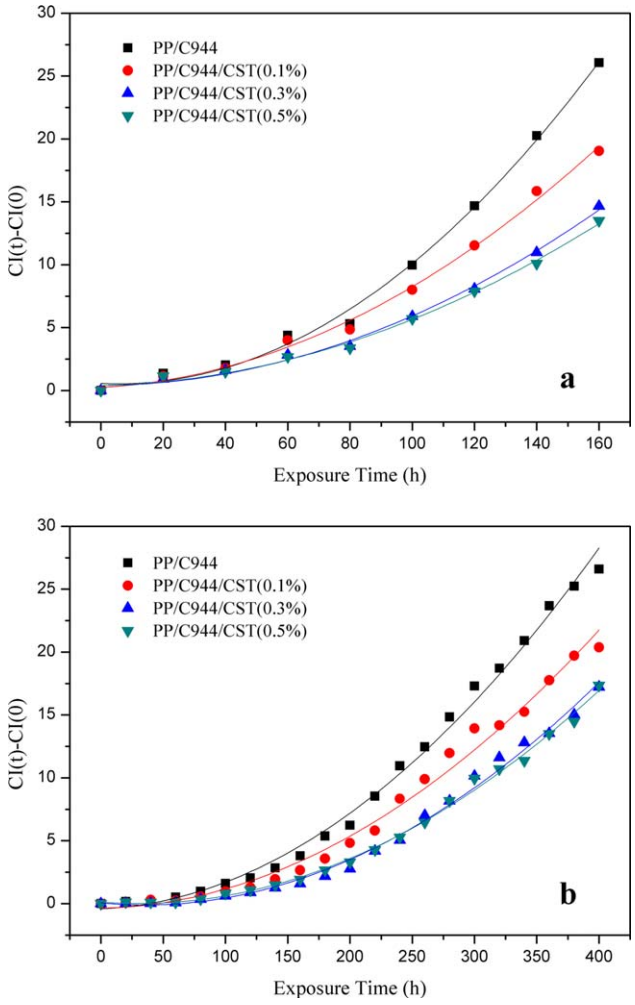

Figure 8. Carbonyl index of PP/C944/CST with different amount of CST under (a) UVC (254 nm) and (b) UVB (302 nm). [Color figure can be viewed in the online issue, which is available at wileyonlinelibrary.com.]

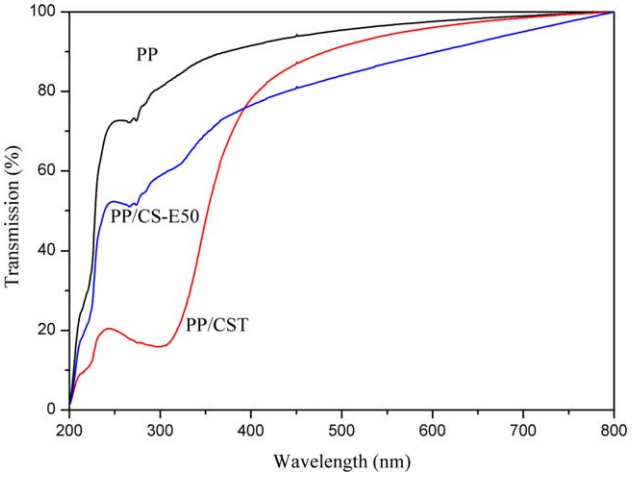

Figure 7. UV–Vis transmission spectra of PP composites (0.5 wt % TiO_2). [Color figure can be viewed in the online issue, which is available at wileyonlinelibrary.com.]

the wavelength shorter than 400 nm, which covered almost the entire range of UV light.[10] The UV absorption of T328 had two strong absorption peaks at about 300 and 350 nm and was relatively weak at other bands. The difference of UV absorption between CST and T328 could explain the results in Figure 10.

In summary, the combination of CST nanorods and C944 is more efficient in the photostabilization of PP. The synergistic effect between the rod-like CST nanoparticles and the C944 was better than the combination of C944 and the spherical CS-E50 nanoparticles. The experimental results indicate the C944/CST combination is even better than the typical C944/T328 system, which is commonly used in the photostabilization of polymers.[47,48]

CONCLUSIONS

In the present work, rutile-type TiO_2 nanorods were prepared and superficially modified and their photostabilization characteristics in PP/TiO_2 nanocomposites was investigated in comparison with spherical TiO_2 nanoparticles and in combination

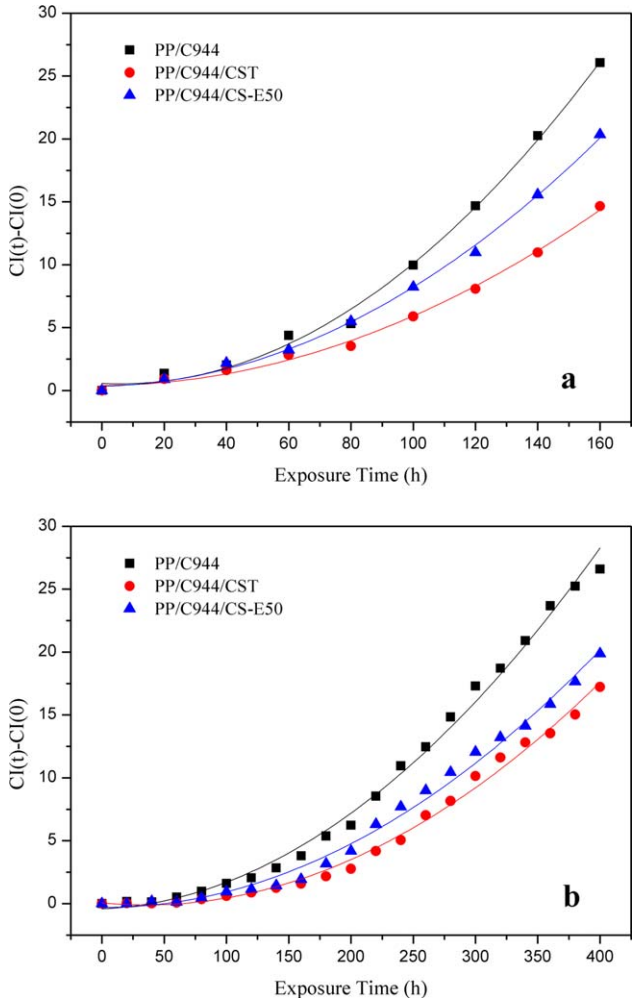

Figure 9. Carbonyl index of PP combinations (0.3 wt % TiO_2 and HALS) under (a) UVC (254 nm) and (b) UVB (302 nm). [Color figure can be viewed in the online issue, which is available at wileyonlinelibrary.com.]

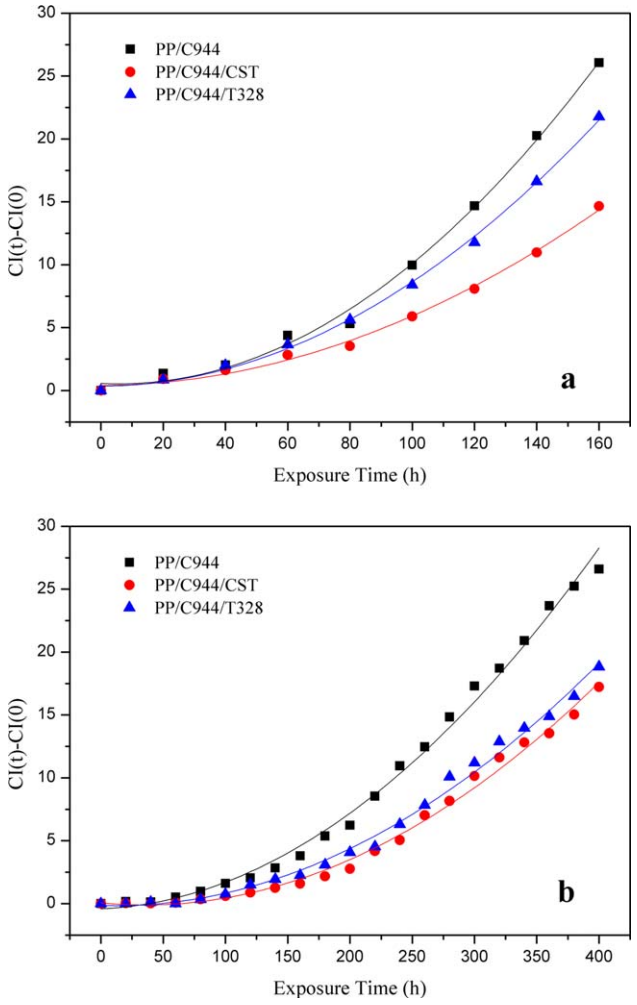

Figure 10. Carbonyl index of PP combinations (0.3 wt % for each additive) under (a) UVC (254 nm) and (b) UVB (302 nm). [Color figure can be viewed in the online issue, which is available at wileyonlinelibrary.com.]

with an HALS light stabilizer. Because of their higher aspect ratio and less agglomeration than the spherical counterpart CS-E50, the calcined silica-coated TiO_2 nanorods CST had larger BET specific surface area, which is representative a larger effective shielding area against the harmful UV radiation in the nanocomposites.

When compounded standalone with the PP matrix, the CST nanorods were well dispersed in the matrix due to the elimination of the hydrophilic active groups during the calcination. The PP/CST film revealed higher photostability as the UV absorption was found covering almost the entire range of UV radiation at a high level, while the UV shielding of PP/CS-E50 was poor. When used in combination with the traditional HALS UV stabilizer C944, a synergistic effect between the nanorods and the HALS was found and the more effective content of CST was 0.3 wt %, which is equal to that of C944 commonly used in PP. By comparison between the PP/C944/CST and PP/C944/T328 systems, the synergistic effect of the CST nanorods was stronger than the organic UV absorber T328 because the UV absorption of the hindered phenol was less efficient and effective mainly at the 300 and 350 nm bands.

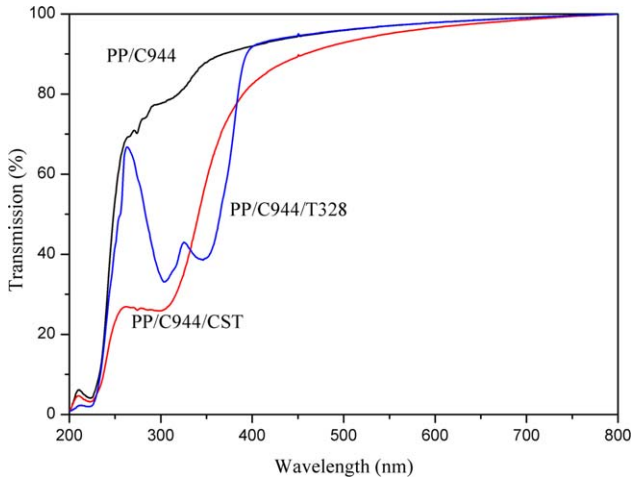

Figure 11. UV–Vis transmission spectra of PP composites films. [Color figure can be viewed in the online issue, which is available at wileyonlinelibrary.com.]

The present work demonstrated the great potential of the rutile-type TiO_2 nanorods in the photostabilization of polymers, especially under the UV radiation of short wavelengths. On one hand, the inorganic CST nanorods are more stable than the conventional organic UV absorbers and resistant to migration and thus could serve with long lifetime. On the other hand, the growing short-wavelength UV radiation on the Earth caused by air pollution would require new and proper additives for the protection of polymer products. It is expected the CST nanorods could find practical applications in the protection of polymers against photodegradation. Intensive research is under progress and will be reported in the future.

ACKNOWLEDGMENTS

This work was financially supported by the National Natural Science Foundation of China (Grant 51133009), the National Basic Research Program of China (Grant No. 2012CB720304) and the "Strategic Priority Research Program" of the Chinese Academy of Sciences (Grant No. XDA09030200).

REFERENCES

1. Pandey, J. K.; Raghunatha Reddy, K.; Pratheep Kumar, A.; Singh, R. P. *Polym. Degrad. Stab.* **2005**, *88*, 234.
2. Ojeda, T.; Freitas, A.; Birck, K.; Dalmolin, E.; Jacques, R.; Bento, F.; Camargo, F. *Polym. Degrad. Stab.* **2011**, *96*, 703.
3. Basfar, A. A.; Ali, K. M. I.; Vaidya, M. M.; Bahamdan, A. A.; Alam, M. A. *Polym. Plast. Technol.* **2010**, *49*, 841.
4. Pospíšil, J.; Nešpurek, S. *Prog. Polym. Sci.* **2000**, *25*, 1261.
5. Horrocks, A. R.; Mwila, J.; Miraftab, M.; Liu, M; Chohan, S. S. *Polym. Degrad. Stab.* **1999**, *65*, 25.
6. Rabello, M. S.; White, J. R. *Polym. Compos.* **1996**, *17*, 691.
7. Kumar, A. P.; Depan, D.; Singh Tomer, N.; Singh R. P. *Prog. Polym. Sci.* **2009**, *34*, 479.
8. Morreale, M.; Dintcheva, N. T.; LaMantia, F. P. *Polym. Int.* **2011**, *60*, 1107.
9. Wang, Z.; Liu, F.; Han, E.; Ke, W.; Luo, S. *Chin. Sci. Bull.* **2009**, *54*, 3464.
10. Mahltig, B.; Böttcher, H.; Rauch, K.; Dieckmann, U.; Nitsche, R.; Fritz, T. *Thin. Solid. Films* **2005**, *485*, 108.
11. Aloui, F.; Ahajji, A.; Irmouli, Y.; George, B.; Charrier, B.; Merlin, A. *Appl. Surf. Sci.* **2007**, *253*, 3737.
12. Li, Y.; Yang, Y.; Fu, S. *Compos. Sci. Technol.* **2007**, *67*, 3465.
13. Zhang, X.; Pi, H.; Guo, S. *J. Appl. Polym. Sci.* **2011**, *122*, 2869.
14. Wen, B.; Wang, F.; Xu, X.; Ding, Y.; Zhang, S.; Yang, M. *Polym. Plast. Technol.* **2011**, *50*, 1375.
15. Caseri, W. *Chem. Eng. Commun.* **2009**, *196*, 549.
16. Patzke, G. R.; Zhou, Y.; Kontic, R.; Conrad, F. *Angew. Chem. Int. Edit.* **2010**, *44*, 2.
17. Chen, X.; Mao, S. S. *Chem. Rev.* **2007**, *107*, 2891.
18. Craig, I. H.; White, J. R. *J. Mater. Sci.* **2006**, *41*, 993.
19. Yang, R.; Christensen, P. A.; Egerton, T. A.; White, J. R.; Maltby, A. *J. Appl. Polym. Sci.* **2011**, *119*, 1330.
20. Kemp, T. J.; McIntyre, R. A. *Polym. Degrad. Stab.* **2006**, *91*, 3020.
21. Kemp, T. J.; McIntyre, R. A. *Polym. Degrad. Stab.* **2006**, *91*, 3010.
22. Chen, X. D.; Wang, Z.; Liao, Z. F.; Mai, Y. L.; Zhang, M. Q. *Polym. Test.* **2007**, *26*, 202.
23. Allen, N. S.; Edge, M.; Ortega, A.; Sandoval, G.; Liauw, C. M.; Verran, J.; Stratton, J.; McIntyre, R. B. *Polym. Degrad. Stab.* **2004**, *85*, 927.
24. Scalarone, D.; Lazzari, M.; Chiantore, O. *Polym. Degrad. Stab.* **2012**, *97*, 2136.
25. Reyes-Coronado, D.; Rodríguez-Gattorno, G.; Espinosa-Pesqueira, M. E.; Cab, C.; de Coss, R.; Oskam, G. *Nanotechnology* **2008**, *19*, 145605.
26. Diebold, U. *Surf. Sci. Rep.* **2003**, *48*, 53.
27. Zeynalov, E. B.; Allen, N. S. *Polym. Degrad. Stab.* **2006**, *91*, 931.
28. Schaller, C.; Rogez, D.; Braig, A. *J. Coat. Technol. Res.* **2008**, *6*, 81.
29. Allen, N. S.; Barcelona, A.; Edge, M.; Wilkinson, A.; Galan Merchan, C.; Ruiz Santa Quiteria, V. *Polym. Degrad. Stab.* **2006**, *91*, 1395.
30. Reingruber, E.; Buchberger, W. *J. Sep. Sci.* **2010**, *33*, 3463.
31. Chen, W.; An, P.; Chen, Y.; Li, Y.; Yan, X.; Chen, L. *Syn. Commun.* **2012**, *42*, 1419.
32. Vaillant, D.; Lacoste, J.; Lemaire, J. *J. Appl. Polym. Sci.* **1997**, *65*, 609.
33. Cao, H.; Yuan, J. P.; Zhang, R.; Huang, C. M.; He, Y.; Sandreczki, T. C.; Jean, Y. C.; Nielsen, B.; Suzuki, R.; Ohdaira, T. *Macromolecules* **1999**, *32*, 5925.
34. Farhadinejad, Z.; Ehsani, M.; Ahmadi-Joneidi, I.; Shayegani, A. A.; Mohseni, H. *IEEE Trans. Dielectr. Electr. Insulat.* **2012**, *19*, 1740.
35. Matsumi, Y.; Kawasaki M. *Chem. Rev.* **2003**, *103*, 4767.
36. Young, A. R. *Br. J. Clin. Pract.* **1997**, *Suppl 89*, 10.
37. Magnaldo, T.; Sarasin, A. *Cells Tissues Organs* **2004**, *177*, 189.
38. Chen, J.; Yang, M. *J. Am. Ceram. Soc.* **2011**, *94*, 3547.
39. Stöber, W.; Fink, A.; Bohn, E. *J. Colloid. Interf. Sci.* **1968**, *26*, 62.
40. Rabello, M. S.; White, J. R. *Polym. Degrad. Stab.* **1997**, *56*, 55.
41. Patterson, A. L. *Phys. Rev.* **1939**, *56*, 978.
42. Henderson, M. A. *Surf. Sci. Rep.* **2002**, *46*, 1.
43. Schoolenberg, G. E. *Polymer* **1991**, *32*, 432.
44. Singh, B.; Sharma, N. *Polym. Degrad. Stab.* **2008**, *93*, 561.
45. Gugumus, F.; Lelli, N. *Polym. Degrad. Stab.* **2001**, *72*, 407.
46. Frank, H. P.; Lehner, H. *J. Polym. Sci. Part C: Polym. Symp.* **1970**, *31*, 193.
47. Liauw, C. M.; Childs, A.; Allen, N. S.; Edge, M.; Franklin, K. R.; Collopy, D. G. *Polym. Degrad. Stab.* **1999**, *65*, 207.
48. Stark, N. M.; Matuana, L. M. *J. Appl. Polym. Sci.* **2003**, *90*, 2609.